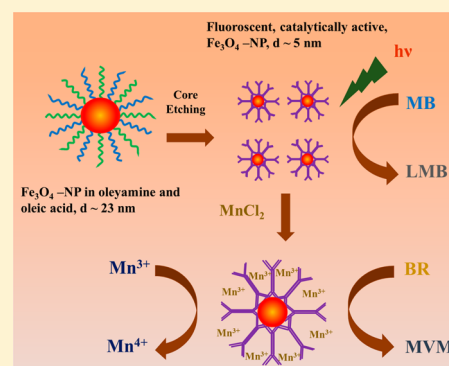# Surface Engineering for Controlled Nanocatalysis: Key Dynamical Events from Ultrafast Electronic Spectroscopy

Nirmal Goswami,[†] Siddhi Chaudhuri,[†] Anupam Giri,[†] Peter Lemmens,[‡] and Samir Kumar Pal*,[†]

[†]Department of Chemical, Biological & Macromolecular Sciences, S. N. Bose National Centre for Basic Sciences, Block JD, Sector III, Salt Lake, Kolkata 700 098, India

[‡]Institute for Condensed Matter Physics, Technical University of Braunschweig, Mendelssohnstr. 3, 38106 Braunschweig, Germany

ABSTRACT: Surface engineering of various nanoparticles (NPs) is of growing interest and an important step to induce/control optical and/or catalytic activities. Although a wide variety of biomedical applications of magnetic Fe_3O_4 NPs in diagnostics as well as therapeutics are well documented, the optical properties of the NPs still remain less well studied. Here we report a top-down fabrication methodology to modify a model ferrofluid with parent NPs sizes ~23 nm, using tartrate as a functionalizing ligand as well as solubilizing agent. The surface engineering involves "ligand exchange" and simultaneous "phase transfer" of Fe_3O_4 NPs (size ~23 nm) from chloroform to water along with subsequent "core etching", resulting in a reduction of particle diameter to ~5 nm. We demonstrate that tartrate-functionalized Fe_3O_4 NPs (T-Fe_3O_4) exhibit ligand to metal charge transfer transition in the UV spectral region, excellent blue luminescence, and efficient reusable photocatalytic activities which are completely absent in the parent NPs. We have used the functionalized NPs for the photodegradation of biomedically important jaundice marker bilirubin in aqueous solution. The surface adsorption of Mn ions on the surface of the T-Fe_3O_4 NPs enables to control the degradation under UV light illumination. While the Mn-adsorbed T-Fe_3O_4 NPs can efficiently degrade bilirubin in dark condition, the activity is significantly reduced under UV light. Finally, the detailed photocatalytic mechanism associated with ultrafast charge and energy transfer process has been discussed. We believe that bilirubin degradation rate can be controlled under UV light by varying Mn ion concentration on the NP's surface which can be a significant advancement for bilirubin degradation study. Overall, the results represent a promising route for the fabrication of Fe_3O_4 NPs adaptable to diverse applications.

1. INTRODUCTION

Magnetite (Fe_3O_4) is a mixed-valence ($Fe^{2+}-Fe^{3+}$) metal oxide, which has been extensively explored in many fields such as magnetic resonance contrast agents, magnetic drug targeting, energy storage, catalysis, etc.[1−6] It has a cubic inverse spinel structure with an electron that can hop between Fe^{2+} and Fe^{3+} ions at room temperature. This allows the formation of efficient catalyst surfaces.[7,8] It is a well-established fact that novel chemical and physical properties originate if the particle sizes are reduced to the nanometer regime. Therefore, synthetic techniques for the preparations of magnetite nanoparticles have been continuously further developed and are topics of ongoing research. Numerous methods have been described to synthesize magnetite nanoparticle such as sol−gel synthesis, hydrothermal, sonochemical, coprecipitation, hydrolysis, thermolysis of precursors, etc.[8−16] Magnetite has also been engineered into a wide range of nanostructures, including uniform nanocrystals, wires, cubes, and hollow nanostructures as well as many others.[8,17−19]

For biological and environmental applications, it is essential to have the particles in an aqueous medium. This can be obtained with proper surface coating and functionalization using organic ligands. However, the synthesis of well-dispersed

Fe_3O_4 NPs without aggregation in aqueous medium showed very limited success. This is because they suffer from limited stability and uniformity due to their high reactivity under ambient conditions as well as large magnetization.[20] In contrast, nonaqueous methods offer a better control over nanoparticles size and shape; therefore, well-dispersed magnetic Fe_3O_4 nanoparticles have been made often in organic solutions.[16,21] Although nonaqueous methods can provide highly monodisperse NPs in scalable amounts, they all have drawbacks with respect to their biological application perspective. Organic surfactant molecules present in the solution for stabilizing the NPs are insoluble in water due to their long hydrophobic chain.

To overcome this problem, only a few ligand exchange methods have been reported that can be used to transfer the particles from organic phases to aqueous solutions.[22−24] For example, Wang et al. have reported a general method to transfer the oleic acid-stabilized NPs into the aqueous phase by using α-cyclodextrin, where size and the morphology of the nanoparticles remain unaltered after the phase transfer.[24] The

properties of the NPs depend on the size as well as functional ligands. It is also important to mention that for mixed valence oxide NPs, while the application in the field of magnetics, catalysis, and biology has been widely studied, their optical properties remain largely unexplored. Previously, our group has explored the emergence of novel optical properties as a result of functionalization in case of La0.67Sr0.33MnO3 (LSMO NP) and Mn3O4 NPs.[25,26] However, until now, there is no such report for the generation of novel optical properties with suitable ligands in the case of Fe_3O_4 NPs. Moreover, in recent times, significant efforts have also been made to study the catalytic/photocatalytic performances of mixed valence NPs.[26,27]

The size of the NPs greatly influences their catalytic behavior. Generally, NP with lower size has higher surface energy and therefore shows higher catalytic activity. Additionally, improved optical properties often lead to better catalytic performance. For example, Mn_3O_4 NPs of ~5 nm size show enhanced catalytic degradation of organic dyes. It has been proven that the oxidation state of Mn ion has a significant role in the catalytic behavior of Mn_3O_4 NPs. Akin to the variable oxidation state of Mn in Mn_3O_4 NPs, Fe_3O_4 NPs also contain Fe ion with variable oxidation state. Thus, small sized functionalized Fe_3O_4 NPs with novel optical properties may provide better catalytic performance compared to larger NPs. Therefore, the development of new strategies to pull out the monodisperse Fe_3O_4 NPs from the organic to the aqueous phase and a following "core etching" to improve the NPs optical properties for better catalytic performance is of great interest and the motive of our study.

Herein, we report a top-down approach to fabricate Fe_3O_4 NPs that is based on a surface modification method followed by a ligand exchange strategy. We have used sodium tartrate as ligand for surface modification of the NPs. It is more environmentally benign and highly soluble in water, and it consists of two −OH and two −COOH groups which allows a complexation with the surface of Fe_3O_4 NPs, therefore leading to a better controlled fabrication process. In our study, we have used ~23 nm Fe_3O_4 NPs protected by oleylamine/oleyl acid, which has been proved to be an effective capping agent in nonaqueous medium, and carried out a surface modification that results to a reduction of particle diameter from ~23 to ~5 nm due to core etching. The surface-modified tartrate-capped Fe_3O_4 NPs (T- Fe_3O_4) have been characterized by various spectroscopic and microscopic techniques. We have observed multiple absorption bands in the UV−vis region that are assigned to ligand to metal charge transfer transitions (LMCT, associated with tartrate−$Fe^{2+/3+}$ interactions). The surface-modified ~5 nm T- Fe_3O_4 NPs show better photocatalytic activity toward a model cationic organic dye (methylene blue, MB) compared with other existing reports. Most importantly, we demonstrate a recycling of the catalyst for many periods, without any significant loss in catalytic activity and selectivity. Control studies with radical scavenger rule out the possibility of radical pathways like reactive oxygen species (ROS) generation. We propose that the MB degradation kinetics follow a Langmuir−Hinshelwood mechanism, with the surface electron transfer evidenced by our ultrafast spectroscopy data.

We have also explored the potential use of the nanoparticle in the treatment of hyperbilirubinemia, a physiological state of high bilirubin level.[27] Bilirubin (BR) is the yellow breakdown product that is formed during the process of heme degradation. An increased BR level in the blood leads to jaundice. Among many conventional treatments, "phototherapy" is the most common method for reducing high BR level. In spite of being inexpensive and easy to use, there is still some reluctance in the use of phototherapy for fear of unknown immediate and/or long-term side effects. As an alternative, researchers have developed various nanocatalysts such as TiO_2, ZnO, and Mn_3O_4 to treat jaundice.[26,28,29] However, photocatalytic degradation of BR cannot be controlled with the existing state-of-the-art photocatalysts, in particular when the particle morphology remains unaltered. To overcome this problem, we have introduced other functionalized NPs, i.e., T- Fe_3O_4 NPs for the degradation of BR under UV light. Through ultrafast spectroscopy, we have demonstrated that UV light induces efficient energy transfer from the T-Fe_3O_4 NPs to the BR leading to efficient BR degradation. In order make the degradation effective and tunable in the presence of light, we have attached Mn ions on the surface of the T-Fe_3O_4 NPs. To the best of our knowledge, this is the first report toward efficient, tunable catalyst through surface functionalization. Like Mn_3O_4 NPs, we have observed that the degradation rate is faster even in the absence of light while Mn ions are attached on the surface of T-Fe_3O_4 NPs. In the presence of light, Mn ions reduce the catalytic efficiency. Picosecond-resolved fluorescence study reveals that the UV light induces the transfer of excited state electrons of the T-Fe_3O_4 NPs to the surface attached Mn^{3+}, and thus the required transformation for the bilirubin degradation, i.e., Mn^{3+} to Mn^{4+}, gets hindered which results in unusual catalytic activity.

2. MATERIALS AND METHODS

Analytical-grade chemicals were used for synthesis without further purification. Sodium tartrate, sodium hydroxide, potassium bromide, bilirubin, and magnesium chloride were obtained from Sigma-Aldrich. Oleylamine/oleyl acid capped ~23 nm Fe_3O_4 NPs were purchased from Ocean NanoTech, LLC (Springdale, AR). Hydrochloric acid was obtained from Merck. Methylene blue was purchased from Carlo Erba. Millipore water was used throughout the experiments.

2.1. Synthesis of ~5 nm T-Fe_3O_4 NPs. First, 0.5 M tartrate solution was prepared using Millipore water. The pH of the solution was then adjusted to ~7 by control addition of 1 M sodium hydroxide (NaOH) solution. 100 μL of ~23 nm Fe_3O_4 NPs (7.7 mg/mL) (Ocean NanoTech, LLC) was added to 4 mL of 0.5 M tartrate solution followed by extensive stirring for 20 h in a cyclomixer. The mixture was centrifuged and the supernatant was taken out for further modification. Next, the pH of the supernatant was adjusted from 7 to 12 by dropwise addition of 1 M sodium hydroxide (NaOH) solution, and the resulting solution was heated at 70 °C with vigorous stirring for 6 h. Finally, the solution became highly luminescent and used for our studies.

2.2. Quantum Yield Calculation. The quantum yield was calculated according to the equation[30]

$$Q = Q_R \left(\frac{I}{I_R}\right)\left(\frac{OD_R}{OD}\right)\left(\frac{n^2}{n_R^2}\right) \tag{1}$$

where Q and Q_R are the quantum yield of the T-Fe_3O_4 NPs and reference (Hoechst 33258 in water), I and I_R are the integrated fluorescence intensities of the T-Fe_3O_4 NPs and reference, OD and OD_R are the optical densities of the T-Fe_3O_4 NPs and reference at the excitation wavelength, and n and n_R are the refractive indices of the T-Fe_3O_4 NPs and reference solutions.
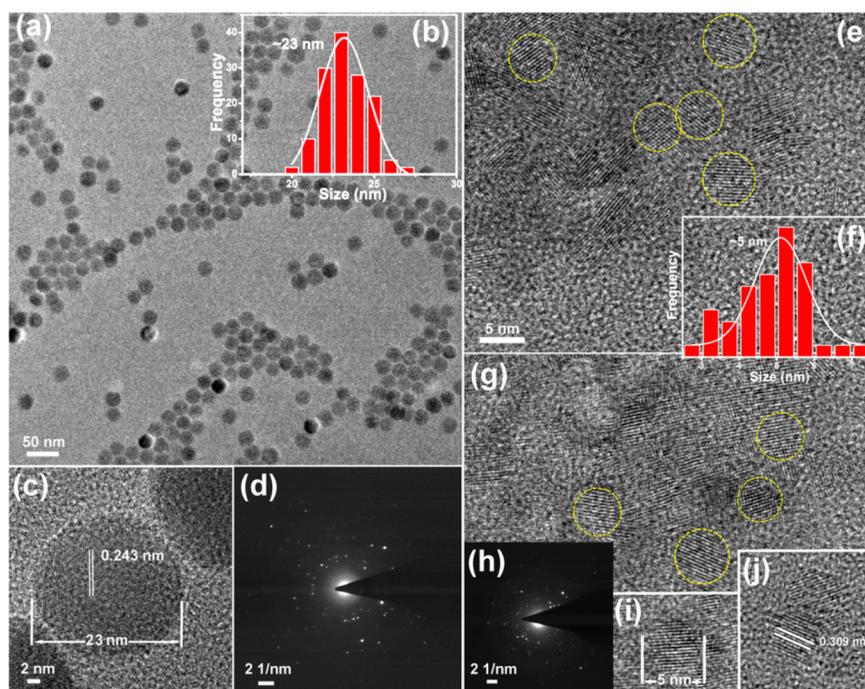
Figure 1. (a) TEM image of ~23 nm Fe_3O_4 NCs before fabrication. (b) Size distribution curve. (c) HRTEM image of single Fe_3O_4 particle showing the (222) plane. (d) SAED patterns of the Fe_3O_4 NPs before fabrication. (e, g) HRTEM images of the Fe_3O_4 NPs after fabrication with tartrate ligand. (f) Size distribution curve showing the average diameter of the NPs is ~5 nm. (h) SAED patterns of the Fe_3O_4 NPs after fabrication. (i) HRTEM image of single ~5 nm Fe_3O_4 particle. (j) (220) plane of T-Fe_3O_4 NPs.

The absolute quantum yield of Hoechst 33258 in water was taken to be 0.034.[31]

2.3. Characterization. The Fe_3O_4 NPs were characterized by high resolution transmission electron microscopy (HRTEM) (FEI TecnaiTF-20). Samples for TEM imaging were prepared by placing a drop of nanoparticle solution on a carbon-coated Cu grid, and the solvent was evaporated under a light bulb. UV–vis absorption spectra were measured with a spectrophotometer (Shimadzu). The characteristic fluorescence excitation and emission spectra were recorded on a Jobin Yvon Model Fluoromax-3 fluorometer. A JASCO FTIR-6300 spectrometer was used to confirm the functionalization of tartrate with the Fe_3O_4 NPs. For FTIR measurements, powdered samples were mixed with KBr powder and pelletized. The background correction was made by using a reference of KBr pellets.

Picosecond-resolved fluorescence decay transients were measured by using a commercially available spectrophotometer (Life Spec-ps, Edinburgh Instruments, UK) with 80 ps instrument response function (IRF). The observed fluorescence transients were fitted by using a nonlinear least-squares fitting procedure to a function ($X(t) = \int_0^t E(t')R(t - t')\, dt'$) comprising of convolution of the IRF ($E(t)$) with a sum of exponential ($R(t) = A + \sum_{i=1}^N B_i e^{-t/\tau_i}$) with pre-exponential factors (B_i), characteristic lifetimes (τ_i), and a background (A). Relative concentration in a multiexponential decay was finally expressed as $c_n = (B_n / \sum_{i=1}^N B_i) \times 100$. The quality of the curve fitting was evaluated by reduced χ^2 and residual data.

In order to measure the UV light-induced degradation processes with spectroscopic precision, a versatile fiber-optic based system was used for sensitive optical measurements. The characteristic absorption of MB at 660 nm and bilirubin at 450 nm were chosen for monitoring the degradation process with T-Fe_3O_4 NPs under UV light with wavelength around 360 nm

at room temperature. The absorption spectra of MB and bilirubin were recorded at 100 s intervals, using SPECTRA SUITE software supplied by Ocean Optics, and finally plotted the MB absorption at 660 nm the bilirubin absorption at 450 nm against the time of photoirradiation.
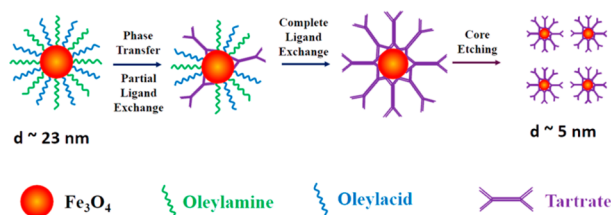
The Förster distances of donor−acceptor pair were calculated using the equation[32] $R_0 = 0.211 \times [\kappa^2 n^{-4} \Phi_D J(\lambda)]^{1/6}$ in angstroms, where, R_0 is the distance between the donor and the acceptor at which the energy transfer efficiency is 50% and κ^2 is a factor which describes the relative orientation in space of the transition dipoles of the donor and acceptor. The magnitude of κ^2 is assumed to be 0.66[32] for random orientation of donor and acceptor pair. The refractive index (n) of the medium (aqueous) is assumed to be 1.33. $J(\lambda)$, the overlap integral, which expresses the degree of spectral overlap between the donor emission and the acceptor absorption, is given by, $J(\lambda) = [\int_0^\infty F_D(\lambda)\varepsilon_A(\lambda)\lambda^4\, d\lambda]/[\int_0^\infty F_D(\lambda)\, d\lambda]$, where $F_D(\lambda)$ is the fluorescence intensity of the donor in the wavelength range of λ to $\lambda + d\lambda$ and is dimensionless. $\varepsilon_A(\lambda)$ is the extinction coefficient (in $M^{-1}\ cm^{-1}$) of the acceptor at λ. If λ is in nm, then $J(\lambda)$ is in units of $M^{-1}\ cm^{-1}\ nm^4$. Once the value of R_0 is known, the donor−acceptor distance (r) is calculated using the formula $r^6 = [R_0^6(1 - E)]/E$, where E is the efficiency of energy transfer, which can be expressed as follows: $E = 1 - \tau_{DA}/\tau_D$, where τ_D and τ_{DA} are lifetimes of the donor in absence and in the presence of the acceptor.

3. RESULTS AND DISCUSSION

3.1. TEM and HRTEM Studies. Figure 1a demonstrates the TEM image of colloidal Fe_3O_4 NPs used for surface modification studies. It is found that the particles are spherical in shape with a narrow size distribution and the average diameter is observed to be ~23 nm (Figure 1b). The high-resolution image shown in Figure 1c confirms the crystallinity

of the NPs. The interplanar distance between the fringes is about 0.243 nm, which corresponds to the distance between (222) planes of the Fe_3O_4 cubic crystal lattice. The highly crystalline nature is further confirmed by selected-area electron diffraction (SAED) analysis (Figure 1d). After successful phase transfer, extensive TEM studies have been carried out in order to characterize the water-soluble tartrate-capped Fe_3O_4 (T-Fe_3O_4) NPs in detail. Figure 1e depicts the HRTEM image of the particles after being fabricated by tartrate ligand. From the micrograph, it is evident that nearly monodisperse ~23 nm Fe_3O_4 NPs have been transformed into spherical NPs with a relatively uniform size distribution having average diameter ~5 nm. The size distribution of the T-Fe_3O_4 NPs is shown in Figure 1f. The SAED pattern (Figure 1g) and the HRTEM image showing lattice fringes (Figure 1h,i) indicate that the fabricated particles are highly crystalline in nature. Although, the lattice fringes observed in T-Fe_3O_4 NPs, which is ~0.309 nm (Figure 1j), is different from the parent Fe_3O_4 particles, indicating that T-Fe_3O_4 NPs are lying on a different plane after fabrication. A plausible mechanism that phase transfer of ~23 nm Fe_3O_4 NPs and their fabrication with tartrate ligand is shown in a schematic diagram (Scheme 1).

Scheme 1. Schematic Representation Showing Stepwise Transformation and Fabrication of ~23 nm Fe_3O_4 NPs by Tartrate Ligand

3.2. UV–Vis, Luminescence, and FTIR Studies.
It is well-known that surface electronic structure of NPs may change due to functionalization of the NPs with organic ligands.[26] Before fabrication with tartrate ligand, we have checked the optical absorption spectrum of Fe_3O_4 NPs in chloroform. As shown in Figure 2a (black curve), it has no such distinct absorption signature in the UV–vis region. However, aqueous solution of T-Fe_3O_4 NPs shows a well-defined absorption spectrum with characteristic peaks in the UV region (Figure 2a). Since tartrate has no such characteristic feature in the UV–vis region, we anticipate that the high-energy bands originate due to the ligand to metal charge transfer transition (LMCT). Apparently, tartrate, having two α-hydroxy carboxylate groups, is considered to be strong field ligand and would preferably coordinate with Fe^{2+}/Fe^{3+} metal ions center on the NPs surface. Therefore, it is expected that both Fe^{2+}/Fe^{3+} will be in the low spin state due to the presence of strong ligand field. Since it is more difficult to reduce Fe^{2+} compared to Fe^{3+}, the LMCT bands involving Fe^{2+} ion are expected to arise in the high energy region, and therefore the bands at 272, 320, and 368 nm are attributed to LMCT to Fe^{2+} ($^1A_{1g} \rightarrow {}^1E_g$), LMCT to Fe^{3+} ($^2T_{2g} \rightarrow {}^2E_g$), and LMCT to Fe^{2+} ($^1A_{1g} \rightarrow {}^1T_{2g}$) in a low-spin octahedral environment.[33,34] Interestingly, after high pH and temperature (at pH ~ 12 and 70 °C for 6 h) treatment, T-Fe_3O_4 NPs show blue luminescence (λ_{em} = 440 nm) upon excitation with 340 nm wavelength. Figure 2b depicts the excitation and emission spectra of T-Fe_3O_4 NPs in aqueous medium. The consistency of the luminescence excitation spectrum with that of the UV–

vis absorption indicates the emission may originate predominantly from the LMCT excited states. Moreover, for 340 nm excitation, the integrated luminescence quantum yield for T-Fe_3O_4 NPs is 0.0056, using Hoechst33258 as the reference. Previously, Govindaiah et al. have reported luminescent Fe_3O_4 NPs protected with the 5-amino-1,10-phenanthroline ligand; however, the origin of luminescence was due to the functionalizing ligand.[35]

In order to get the direct evidence of ligand functionalization onto the surface of NPs, FTIR spectra (Figure 2c) of both tartrate and T-Fe_3O_4 NPs exhibit a broad peak from 3400 to 3600 cm^{-1}, which originates due to the stretching vibration of the hydroxyl groups of tartrate ligand. Pure tartrate has peaks at 3201 and 3460 cm^{-1}, which become shifted to 3205 and 3454 cm^{-1} upon functionalization with Fe_3O_4 NPs, clearly confirming the binding of ligands with NPs surface. It is well-known that Fe_3O_4 has a characteristic Fe–O vibration band at around 580 cm^{-1}.[36] However, in our case we do not observe such a band probably because of the high concentration of tartrate ligand. Figure 2d reveals the picosecond-resolved luminescence decay transients of the T-Fe_3O_4 NPs upon excitation with 375 nm laser. Lifetime values are obtained by the multiexponential fitting of the luminescence at 440 nm. Time components are 580 ps (45%) and 3.95 ns (55%). The short average lifetime (2.45 ns) is in agreement with spin-allowed transition and consistent with the previous values on the luminescence lifetime originated from LMCT.[37]

4. PHOTOCATALYSIS

4.1. Photodegradation of Methylene Blue.
After examining the optical and structural characteristics of T-Fe_3O_4 NPs, to take full advantage of their photoluminescence properties, we have performed detail photocatalytic measurements under UV light. We have selected methylene blue (MB) as a model probe for photocatalytic experiment. It is a potent cationic dye used in the textile industry, with maximum absorption of light around 660 nm. The peak has been used to monitor the concentration of MB during the photocatalytic degradation measurements. The detailed experimental procedure has been given in the experimental section. As a control study, we have tested the photocatalytic properties of tartrate and as-prepared T-Fe_3O_4 NPs under UV light. However, the peak intensity at 660 nm remains almost unchanged even after 120 min in both cases. Later on, we have examined the photocatalytic behavior of luminescent T-Fe_3O_4 NPs under similar experimental condition and observed unprecedented photocatalytic behavior. As the rate of a catalytic reaction depends on factors like concentration and surface area of the catalyst, therefore, we have studied catalyst concentration dependent kinetics. From Figure 3a, it has been found that the rate of the reaction increases with increase of the catalyst concentration. It is obvious for a surface catalysis reaction because increase in catalyst concentration means more surface area available for effective catalysis. It can also be seen that degradation of MB followed an "induction period" and subsequent "acceleration period". Note that earlier reports on Fe_3O_4 NPs suggest that MB undergoes degradation process instantaneously after the exposure of UV light. However, induction time has been reported for TiO_2-mediated photocatalysis.[38] We propose that during the induction period buildup of reaction intermediates occurs, and the surface of the NPs becomes saturated with the MB molecules. As revealed from Figure 3a, the induction time becomes shorter with
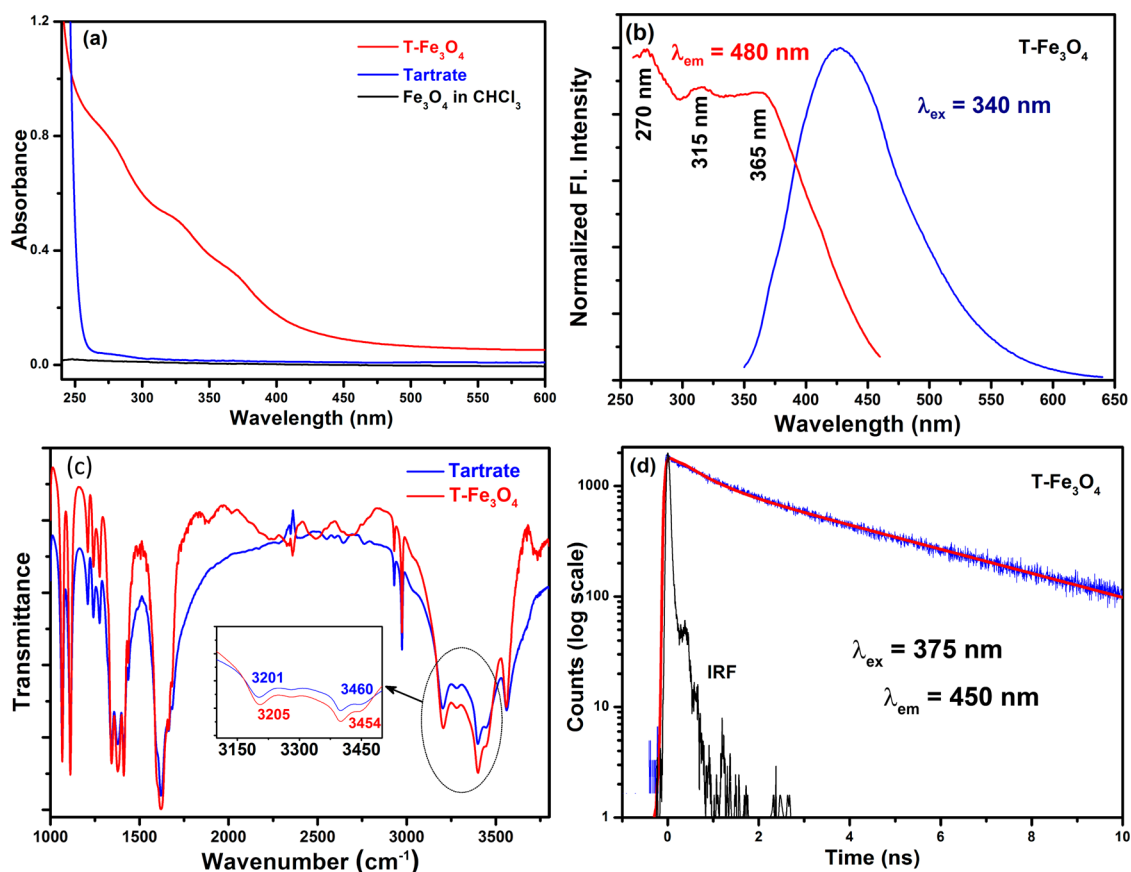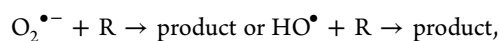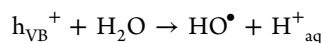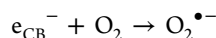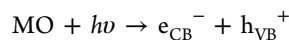
Figure 2. (a) UV−vis absorption spectra of ∼23 nm Fe_3O_4 NPS in chloroform (black), tartrate (blue), and T-Fe_3O_4 NPs (red) in aqueous medium. (b) Excitation and emission spectra of T-Fe_3O_4 NPs. (c) FTIR spectra of tartrate (blue) and T-Fe_3O_4 NPs (red). The −OH region of the spectra has been shown in the inset. (d) Picosecond-resolved fluorescence transient of aqueous T-Fe_3O_4 solution.

increase of NPs concentration in a fixed concentrated aqueous MB solution of pH 5. Furthermore, to confirm the stability of the high photocatalytic performance of the T-Fe_3O_4 NPs, recycling experiments have been conducted. We have carried out five consecutive cycles (Figure 3b) that show that the rate of the photocatalytic degradation remains almost constant, indicating the high stability of the catalyst even under long time UV exposure. This observation indicates that the catalytic properties of the T-Fe_3O_4 NPs become rejuvenated after each cycle. This finding is especially important for its industrial application. Figure 3b depicts that in the first cycle, the excellent photocatalytic activity (90% MB degradation) is obtained in the presence of very small amount of T-Fe_3O_4 NPs (0.025 mg/mL), and the degradation becomes 65% after fifth cycle. The results demonstrate that these T-Fe_3O_4 NPs can indeed serve as highly effective and convenient recyclable photocatalyst.

Often the question for the mechanism involved in photocatalysis. It is well-known that different photocatalytic pathways have been established for the degradation of organic dyes.[39,40] Here, we first consider the approach which is based on the generation of reactive oxygen species (ROS). The presence of strong UV light excites electron from the valence band (VB) to the conduction band (CB) of the metal oxide (MO), leaving a positively charged hole in the VB. The electron in the CB and the hole in the VB then reacts with O_2 and H_2O on the MO surface, therefore generating reactive oxygen species (ROS) such as $O_2^{\bullet-}$ and $HO^\bullet$. The mechanistic pathway is[41]

$$MO + h\upsilon \rightarrow e_{CB}^- + h_{VB}^+$$

$$e_{CB}^- + O_2 \rightarrow O_2^{\bullet-}$$

$$h_{VB}^+ + H_2O \rightarrow HO^\bullet + H^+_{aq}$$

$$O_2^{\bullet-} + R \rightarrow \text{product or } HO^\bullet + R \rightarrow \text{product,}$$

where R is reactant

The generation of ROS and subsequent radical chain reactions result in the degradation of organic dye. As the fabricated T-Fe_3O_4 NPs exhibit absorption bands in the UV−vis region, the presence of strong UV light may generate ROS. So, the mechanism as explained above is highly possible here. If so, then the rate of photocatalytic degradation is expected to be slow down in the presence of ethanol, which is a well-known radical scavenger. However, as shown in Figure 3c, the catalytic rate of MB degradation remains almost same in the presence and absence of ethanol, which rules out the role of ROS generation in the photocatalytic process. However, the kinetic behavior of MB degradation can be described by the Langmuir−Hinshelwood (LH) model.[42,43] The generalized LH model can be expressed as

$$R = \frac{dC_0}{dt} = k_S S C_0 = \frac{k_S S k_0 C_0}{1 + k_0 C_0}$$

where, R is the rate of the reaction, k_S is the rate constant of the reaction, C_0 is the initial concentration of the MB in water, k_0 is the adsorption constant for MB molecules, and S is the surface
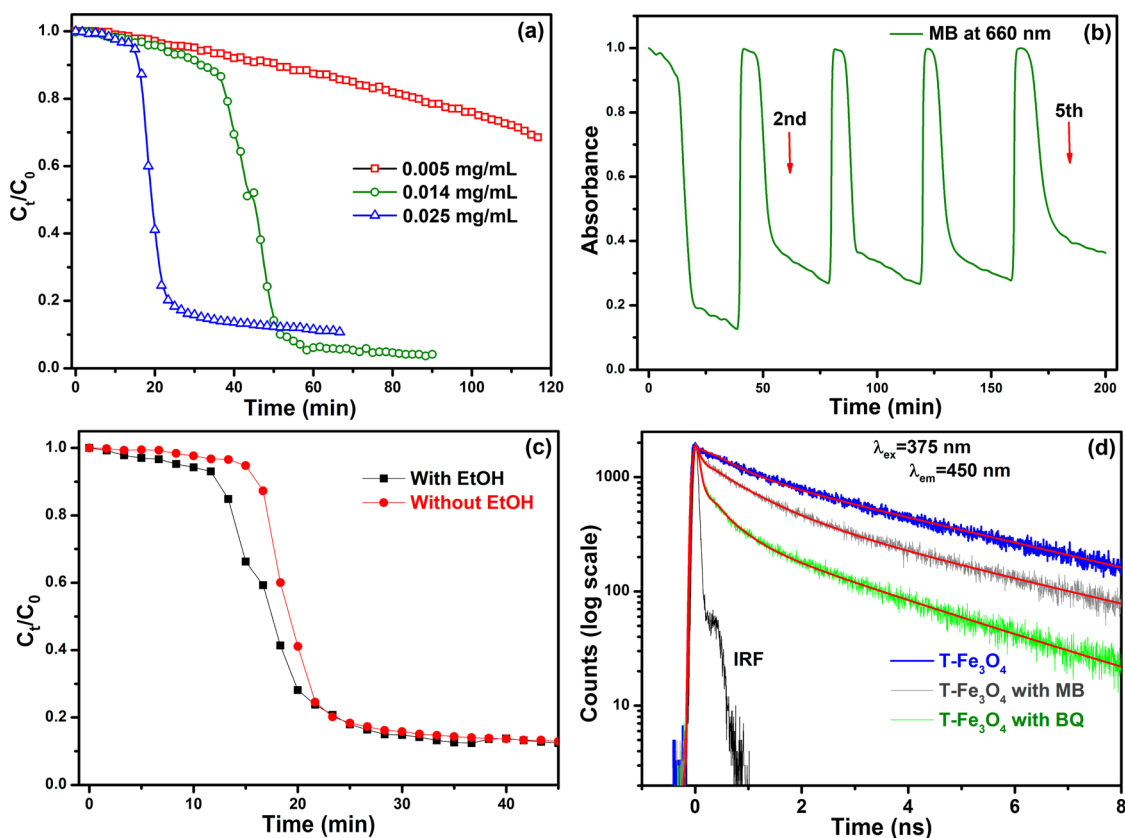
Figure 3. (a) Photocatalytic degradation of fixed concentrated methylene blue solution with various amounts of T-Fe$_3$O$_4$ NPs. (b) Cycling curve of photocatalytic degradation of methylene blue in the presence of fixed concentration (0.025 mg/mL) of Fe$_3$O$_4$ NPs. (c) Photocatalytic degradation of methylene blue by T-Fe$_3$O$_4$ NPs in presence and absence of ethanol. Concentration of T-Fe$_3$O$_4$ NPs = 0.025 mg/mL. (d) Picosecond-resolved fluorescence decay transients of T-Fe$_3$O$_4$ NPs in the absence and presence of methylene blue and benzoquinone.

area of the T-Fe$_3$O$_4$ NPs. Since MB has very high adsorption, so the rate is proportional to the surface area (S) of the NPs present in the system. The rate constant values are found to be increasing with the increase in concentration of T-Fe$_3$O$_4$ NPs, suggesting zero-order dependence of the reaction rate on surface area.

As discussed above, the surface interaction between MB and T-Fe$_3$O$_4$ NPs is confirmed, and the enhanced photocatalytic activity could be explained by the following mechanism: it is well-known that electron transfer is associated with the MB degradation.[44] As T-Fe$_3$O$_4$ NPs have good photoluminescence properties upon excitation with UV light, photoinduced electron transfer (PET) may possibly account to the degradation process. In order to unravel that, we have performed picosecond-resolved fluorescence studies (Figure 3d), which directs significant quenching of the decay transient of T-Fe$_3$O$_4$ NPs upon complexation with MB molecules. As a control study, we have considered the complexation of the T-Fe$_3$O$_4$ NPs with an organic molecule, benzoquinone (BQ), which is a well-known as an electron acceptor and efficiently accepts excited electrons from the nanosurface.[45] In the presence of BQ, a very sharp decay (monitored at 450 nm) is observed, which is associated with the PET process (Figure 3d). It can be seen from Table 1 that the T-Fe$_3$O$_4$ NPs in the presence of MB exhibit an ultrafast time component of 75 ps with a majority (57%) which is akin to the component, i.e., 45 ps (83%) in the presence of BQ, at the same excitation of 375 nm. The result implies the favorable PET process from the T-Fe$_3$O$_4$ NPs to the MB molecules at the surface of the NPs.

Table 1. Lifetime Values T-Fe$_3$O$_4$ NPs in the Absence and Presence of BQ, MB, Mn Ions, and BR[a]

system	τ_1	τ_2	τ_3	τ_{av}
T-Fe$_3$O$_4$		580 ps (45%)	3.95 ns (55%)	2.45 ns
T-Fe$_3$O$_4$ + BQ	45 ps (83%)	395 ps (10%)	2.60 ns (07%)	235 ps
T-Fe$_3$O$_4$ + MB	75 ps (57%)	930 ps (27%)	3.95 ns (16%)	950 ps
T-Fe$_3$O$_4$ + Mn ions	75 ps (64%)	707 ps (24%)	3.06 ns (12%)	0.60 ns
T-Fe$_3$O$_4$ + BR	25 ps (38%)	470 ps (43%)	3.92 ns (19%)	0.98 ns

[a]Numbers in parentheses indicate relative percentage. λ_{em} = 450 nm, λ_{ex} = 375 nm. Standard error ∼5%.

4.2. Controlled Photodegradation of Bilirubin. Following the photocatalytic degradation of MB, we have examined the potential of modified T-Fe$_3$O$_4$ NPs toward the degradation of bilirubin (BR). The characteristic absorbance band of BR at 450 nm has been chosen for monitoring the kinetic study using UV–vis spectroscopy. Figure 4a shows the relative concentration (C_t/C_0) of BR with respect to the UV irradiation time. In the absence of UV light, we observe almost minimal degradation which depicts the different behavior of Fe^{2+}/Fe^{3+} system compared to Mn^{3+}/Mn^{4+} system in Mn$_3$O$_4$ NPs which can efficiently degrade BR in dark conditions. However, T-Fe$_3$O$_4$ NPs can effectively degrade BR (30%) in the presence of UV light. As the optical absorption spectrum of BR overlaps with the emission of T-Fe$_3$O$_4$ NPs (Figure 4b), we propose
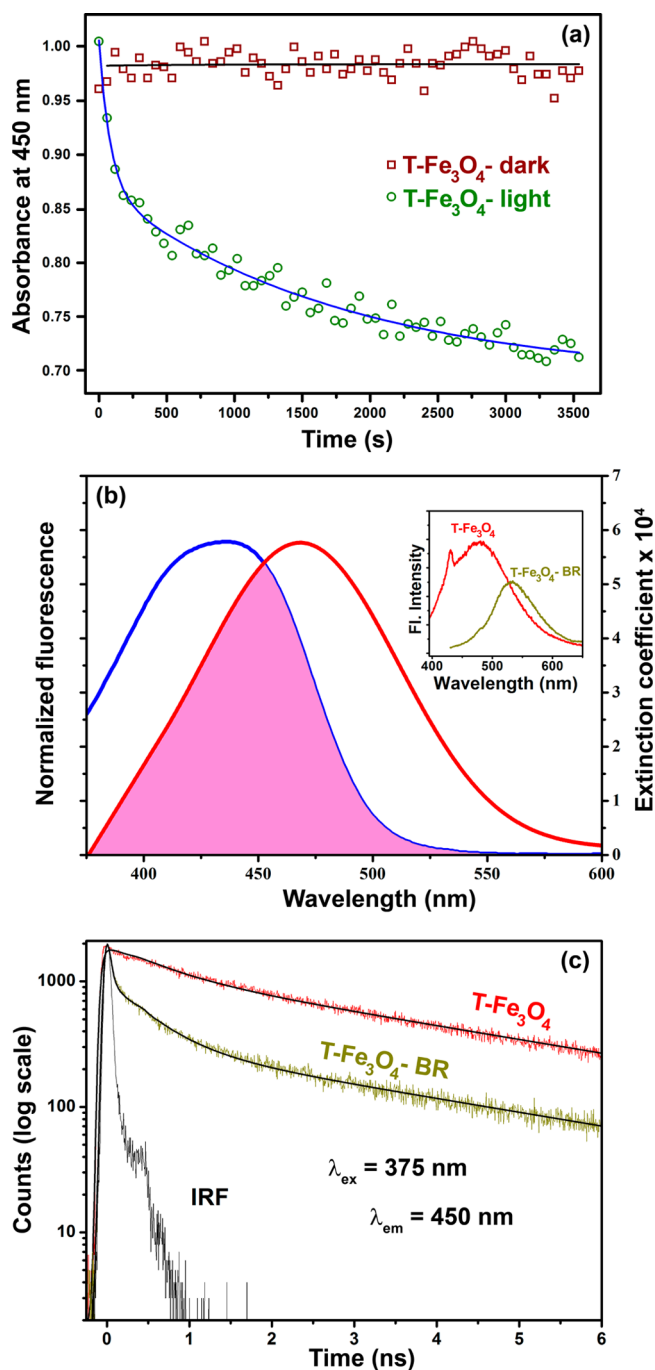
Figure 4. (a) Absorption kinetics of bilirubin (degradation monitored at 450 nm) under UV light as well as in dark in absence and presence of T-Fe₃O₄. (b) Spectral overlap of T-Fe₃O₄ emission and bilirubin absorption. Inset shows steady state emission spectra of the NPs before and after bilirubin addition. (c) Fluorescence lifetime quenching of T-Fe₃O₄ in water in the absence and presence of bilirubin.

FRET from T-Fe₃O₄ NPs (donor) to BR (acceptor) is responsible for the observed degradation. Picosecond-resolved fluorescence spectroscopy is a useful technique that provides information about the excited-state dynamics. The decay transients of T-Fe₃O₄ NPs in aqueous medium in absence (donor) and presence of BR (donor–acceptor) have been shown in Figure 4c. The decay transient of the donor has been fitted with two components, with an average lifetime of 2.45 ns.

The fluorescence decay trace of the donor–acceptor could be fitted with a fast component, apparently corresponding to some nonradiative channel, along with two other components. The details of the numerical fitting of the fluorescence transients are tabulated in Table 1. From the fitting result, we have estimated the Förster distance to be 19.44 Å. The short donor–acceptor distance indicates that BR molecules are in close proximity of the surface of the NPs. It has to be noted that FRET-based efficient BR degradation by ZnO NPs was reported previously.[28]

However, in the present study, the degradation efficiency is lower compared to other reports. Therefore, in order to enhance the degradation rate, we have incorporated Mn ions on the NPs surface. After the addition of MnCl₂, the T-Fe₃O₄ NPs solution has been heated at high temperature for 6 h at pH 12. It is noteworthy to mention that at high pH all the Mn²⁺ will be converted to Mn³⁺. The attachment has been confirmed by the absorption spectroscopy (Figure 5a). The observed peaks around 430 and 565 nm exist due to the d–d transition of Mn³⁺ ion on the NPs surface. After attachment, we have tested the Mn³⁺ attached T-Fe₃O₄ NPs for the degradation of bilirubin. The degradation kinetics with Mn³⁺ attached T-Fe₃O₄ NPs in absence and presence of light has been shown in Figure 5b. It can be seen that BR degradation is much faster in the absence of light. However, the rate is similar to T-Fe₃O₄ NPs in the presence of light. It is well-known that Mn₃O₄ NPs can catalytically degrade BR in the absence of light. It has been proposed that upon addition of bilirubin Mn³⁺ ions in the surface will be converted to Mn⁴⁺ state which generates few reactive oxygen species (ROS) that ultimately degrade bilirubin. In the case of Mn³⁺ attached T-Fe₃O₄ NPs, we propose the similar mechanism for the BR degradation in the absence of light. In the presence of light, Mn³⁺ has a negligible effect which indicates that UV light blocks the Mn³⁺ to Mn⁴⁺ conversion. Thus, the only possibility is the excited state electron transfer from T-Fe₃O₄ NPs to Mn³⁺ ions. Here, we observed the electron transfer in the excited state. Picosecond-resolved fluorescence transients of T-Fe₃O₄ NPs in aqueous medium in the absence and presence of Mn³⁺ ions have been shown in Figure 5c. An electron from T-Fe₃O₄ NPs is transferred to of Mn³⁺ which results in a faster component in the fluorescence lifetime. The details of the numerical fitting of the fluorescence transients are tabulated in Table 1. There are few studies which report that Fe₃O₄ NPs block electron transfer in an electrochemical process.[46,47] The results described in this study indicate that the excited state electron of T-Fe₃O₄ NPs prevents the conversion of Mn³⁺ to Mn⁴⁺ which are attached on its surface leading to slower catalytic rate.

5. CONCLUSION

We have successfully demonstrated a facile top-down approach to fabricate a commercially available ferrofluid using tartrate ligand. Oleic amine/oleyl acid capped ~23 nm Fe₃O₄ NPs have been efficiently phase transferred into aqueous phase from chloroform. The controlled tartrate etching process in aqueous solution converts the particle diameter from 23 to ~5 nm. LMCT optical bands in the electronic spectra enable the elucidation of the quantum origins of excellent blue luminescence. When evaluated for their possible use in photocatalysis, the fabricated T-Fe₃O₄ NPs exhibit a significantly improved performance compared to the reports in the existing literature. The rejuvenating catalytic properties of T-Fe₃O₄ NPs have been illustrated, which reveals the particle as a
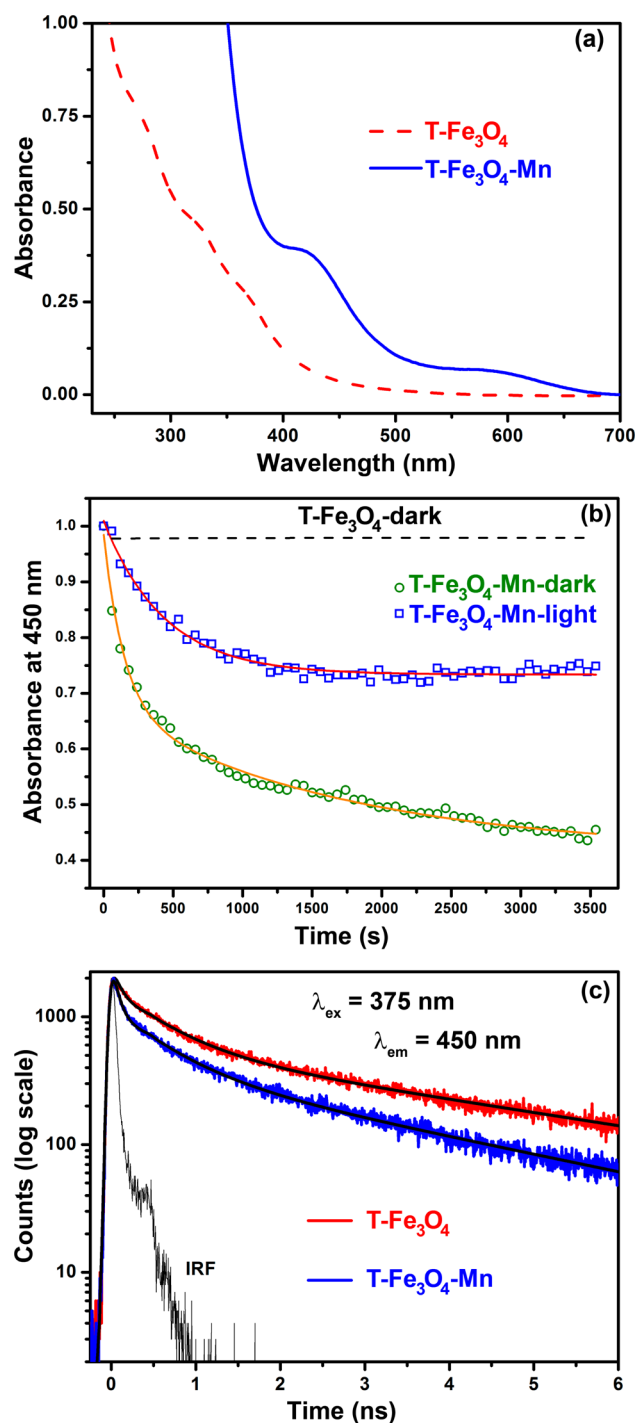
23440

dx.doi.org/10.1021/jp507456n | J. Phys. Chem. C 2014, 118, 23434–23442

Figure 5. (a) UV−vis absorption spectra of T-Fe$_3$O$_4$ NPs in the absence (red) and presence (blue) of manganese ion in aqueous medium. (b) Absorption kinetics of bilirubin (degradation monitored at 450 nm) under UV light as well as in dark in the absence and presence of T-Fe$_3$O$_4$-Mn. (c) Picosecond-resolved fluorescence transients of aqueous T-Fe$_3$O$_4$ solution in the absence and presence of manganese ion.

recyclable and a highly efficient photocatalyst. The results indicate that ROS generation pathway is not the case here; rather, it follows the Langmuir−Hinshelwood model. The catalytic degradation rate for the bilirubin has been accelerated in the absence of UV light when the surface of the T-Fe$_3$O$_4$ NPs has been modified with Mn ions. However, in the presence

of UV light, the degradation is slower due to the blockage of Mn^{3+} to Mn^{4+} transformation through the excited state electron transfer from T-Fe$_3$O$_4$ NPs to the Mn^{3+} ion. This result has importance in direct therapeutic applications against hyperbilirubinemia. We believe that the method described in this study might be extended to other magnetic transition metal oxide nanoparticles which will effectively lead to the development of multifunctional nanomaterials having excellent optical, magnetic, and catalytic properties.

■ **AUTHOR INFORMATION**

Corresponding Author
*E-mail: skpal@bose.res.in (S.K.P.).

Author Contributions
N.G. and S.C. contributed equally to this work.

Notes
The authors declare no competing financial interest.

■ **REFERENCES**

(1) Jun, Y.-w.; Huh, Y.-M.; Choi, J.-s.; Lee, J.-H.; Song, H.-T.; Sungjun, K.; Yoon, S.; Kim, K.-S.; Shin, J.-S.; et al. Nanoscale Size Effect of Magnetic Nanocrystals and Their Utilization for Cancer Diagnosis via Magnetic Resonance Imaging. *J. Am. Chem. Soc.* **2005,** 127, 5732−5733.

(2) Cao, S.-W.; Zhu, Y.-J.; Ma, M.-Y.; Li, L.; Zhang, L. Hierarchically Nanostructured Magnetic Hollow Spheres of Fe$_3$O$_4$ and γ-Fe$_2$O$_3$: Preparation and Potential Application in Drug Delivery. *J. Phys. Chem. C* **2008,** 112, 1851−1856.

(3) Veiseh, O.; Gunn, J. W.; Zhang, M. Design and fabrication of magnetic nanoparticles for targeted drug delivery and imaging. *Adv. Drug Delivery Rev.* **2010,** 62, 284−304.

(4) Li, B.; Cao, H.; Shao, J.; Qu, M.; Warner, J. H. Superparamagnetic Fe$_3$O$_4$ nanocrystals@graphene composites for energy storage devices. *J. Mater. Chem.* **2011,** 21, 5069−5075.

(5) Zeng, T.; Chen, W.-W.; Cirtiu, C. M.; Moores, A.; Song, G.; Li, C.-J. Fe$_3$O$_4$ nanoparticles: a robust and magnetically recoverable catalyst for three-component coupling of aldehyde, alkyne and amine. *Green Chem.* **2010,** 12, 570−573.

(6) Lim, C. W.; Lee, I. S. Magnetically recyclable nanocatalyst systems for the organic reactions. *Nano Today* **2010,** 5, 412−434.

(7) Soeya, S.; Hayakawa, J.; Takahashi, H.; Ito, K.; Yamamoto, C.; Kida, A.; Asano, H.; Matsui, M. Development of half-metallic ultrathin Fe$_3$O$_4$ films for spin-transport devices. *Appl. Phys. Lett.* **2002,** 80, 823−825.

(8) Sun, S. H.; Zeng, H. Size-controlled synthesis of magnetite nanoparticles. *J. Am. Chem. Soc.* **2002,** 124, 8204−8205.

(9) Lemine, O. M.; Omri, K.; Zhang, B.; El Mir, L.; Sajieddine, M.; Alyamani, A.; Bououdina, M. Sol−gel synthesis of 8 nm magnetite (Fe$_3$O$_4$) nanoparticles and their magnetic properties. *Superlattices Microstruct.* **2012,** 52, 793−799.

(10) Daou, T. J.; Pourroy, G.; Bégin-Colin, S.; Grenèche, J. M.; Ulhaq-Bouillet, C.; Legaré, P.; Bernhardt, P.; Leuvrey, C.; Rogez, G.

Hydrothermal Synthesis of Monodisperse Magnetite Nanoparticles. *Chem. Mater.* **2006**, *18*, 4399−4404.

(11) Shafi, K. V. P. M.; Ulman, A.; Yan, X.; Yang, N.-L.; Estournès, C.; White, H.; Rafailovich, M. Sonochemical Synthesis of Functionalized Amorphous Iron Oxide Nanoparticles. *Langmuir* **2001**, *17*, 5093−5097.

(12) Fried, T.; Shemer, G.; Markovich, G. Ordered Two-Dimensional Arrays of Ferrite Nanoparticles. *Adv. Mater.* **2001**, *13*, 1158−1161.

(13) Iida, H.; Takayanagi, K.; Nakanishi, T.; Osaka, T. Synthesis of Fe_3O_4 nanoparticles with various sizes and magnetic properties by controlled hydrolysis. *J. Colloid Interface Sci.* **2007**, *314*, 274−280.

(14) Yu, W. W.; Falkner, J. C.; Yavuz, C. T.; Colvin, V. L. Synthesis of monodisperse iron oxide nanocrystals by thermal decomposition of iron carboxylate salts. *Chem. Commun.* **2004**, 2306−2307.

(15) Hyeon, T.; Lee, S. S.; Park, J.; Chung, Y.; Na, H. B. Synthesis of Highly Crystalline and Monodisperse Maghemite Nanocrystallites without a Size-Selection Process. *J. Am. Chem. Soc.* **2001**, *123*, 12798−12801.

(16) Laurent, S.; Forge, D.; Port, M.; Roch, A.; Robic, C.; Vander Elst, L.; Muller, R. N. Magnetic Iron Oxide Nanoparticles: Synthesis, Stabilization, Vectorization, Physicochemical Characterizations, and Biological Applications. *Chem. Rev.* **2008**, *108*, 2064−2110.

(17) Yang, H. T.; Ogawa, T.; Hasegawa, D.; Takahashi, M. Synthesis and magnetic properties of monodisperse magnetite nanocubes. *J. Appl. Phys.* **2008**, 103.

(18) Gao, G.; Liu, X.; Shi, R.; Zhou, K.; Shi, Y.; Ma, R.; Takayama-Muromachi, E.; Qiu, G. Shape-Controlled Synthesis and Magnetic Properties of Monodisperse Fe_3O_4 Nanocubes. *Cryst. Growth Des.* **2010**, *10*, 2888−2894.

(19) Peng, S.; Sun, S. Synthesis and Characterization of Monodisperse Hollow Fe_3O_4 Nanoparticles. *Angew. Chem., Int. Ed.* **2007**, *46*, 4155−4158.

(20) Wu, W.; He, Q. G.; Jiang, C. Z. Magnetic Iron Oxide Nanoparticles: Synthesis and Surface Functionalization Strategies. *Nanoscale Res. Lett.* **2008**, *3*, 397−415.

(21) Si, S.; Li, C.; Wang, X.; Yu, D.; Peng, Q.; Li, Y. Magnetic Monodisperse Fe_3O_4 Nanoparticles. *Cryst. Growth Des.* **2005**, *5*, 391−393.

(22) Yu, W. W.; Chang, E.; Sayes, C. M.; Drezek, R.; Colvin, V. L. Aqueous dispersion of monodisperse magnetic iron oxide nanocrystals through phase transfer. *Nanotechnology* **2006**, *17*, 4483−4487.

(23) Zhang, T.; Ge, J.; Hu, Y.; Yin, Y. A General Approach for Transferring Hydrophobic Nanocrystals into Water. *Nano Lett.* **2007**, *7*, 3203−3207.

(24) Wang, Y.; Wong, J. F.; Teng, X.; Lin, X. Z.; Yang, H. "Pulling" Nanoparticles into Water: Phase Transfer of Oleic Acid Stabilized Monodisperse Nanoparticles into Aqueous Solutions of α-Cyclodextrin. *Nano Lett.* **2003**, *3*, 1555−1559.

(25) Giri, A.; Goswami, N.; Bootharaju, M. S.; Xavier, P. L.; John, R.; Thanh, N. T. K.; Pradeep, T.; Ghosh, B.; Raychaudhuri, A. K.; Pal, S. K. Emergence of Multicolor Photoluminescence in $La_{0.67}Sr_{0.33}MnO_3$ Nanoparticles. *J. Phys. Chem. C* **2012**, *116*, 25623−25629.

(26) Giri, A.; Goswami, N.; Pal, M.; Zar Myint, M. T.; Al-Harthi, S.; Singha, A.; Ghosh, B.; Dutta, J.; Pal, S. K. Rational surface modification of Mn_3O_4 nanoparticles to induce multiple photoluminescence and room temperature ferromagnetism. *J. Mater. Chem. C* **2013**, *1*, 1885−1895.

(27) Giri, A.; Goswami, N.; Sasmal, C.; Polley, N.; Majumdar, D.; Sarkar, S.; Bandyopadhyay, S. N.; Singha, A.; Pal, S. K. Unprecedented catalytic activity of Mn_3O_4 nanoparticles: potential lead of a sustainable therapeutic agent for hyperbilirubinemia. *RSC Adv.* **2014**, *4*, 5075−5079.

(28) Bora, T.; Lakshman, K. K.; Sarkar, S.; Makhal, A.; Sardar, S.; Pal, S. K.; Dutta, J. Modulation of defect-mediated energy transfer from ZnO nanoparticles for the photocatalytic degradation of bilirubin. *Beilstein J. Nanotechnol.* **2013**, *4*, 714−725.

(29) Hall, J. B.; Dobrovolskaia, M. A.; Patri, A. K.; McNeil, S. E. Characterization of nanoparticles for therapeutics. *Nanomedicine* **2007**, *2*, 789−803.

(30) Goswami, N.; Makhal, A.; Pal, S. K. Toward an Alternative Intrinsic Probe for Spectroscopic Characterization of a Protein. *J. Phys. Chem. B* **2010**, *114*, 15236−15243.

(31) Hard, T.; Fan, P.; Kearns, D. R. A Fluorescence Study of the Binding of Hoechst-33258 and Dapi to Halogenated Dnas. *Photochem. Photobiol.* **1990**, *51*, 77−86.

(32) Lakowicz, J. R. *Principles of Fluorescence Spectroscopy*; Kluwer Academic/Plenum: New York, 2006.

(33) Templeton, D. *Molecular and Cellular Iron Transport*; Taylor and Francis: London, 2002; p 848.

(34) Sherman, D. M. Electronic spectra of Fe^{3+} oxides and oxide hydroxides in the near IR to near UV. *Am. Mineral.* **1985**, *70*, 1262−1269.

(35) Govindaiah, P.; Park, T. J.; Jung, Y. J.; Lee, S. J.; Ryu, D. Y.; Kim, J. H.; Cheong, I. W. Luminescent iron oxide nanoparticles prepared by one-pot aphen-functionalization. *Macromol. Res.* **2010**, *18*, 1109−1114.

(36) Yang, K.; Peng, H.; Wen, Y.; Li, N. Re-examination of characteristic FTIR spectrum of secondary layer in bilayer oleic acid-coated Fe_3O_4 nanoparticles. *Appl. Surf. Sci.* **2010**, *256*, 3093−3097.

(37) Vogler, A.; Kunkely, H. Luminescence from Hexacyanoruthenate(III). *Inorg. Chim. Acta* **1981**, *53*, L215−L216.

(38) Virkutyte, J.; Baruwati, B.; Varma, R. S. Visible light induced photobleaching of methylene blue over melamine-doped TiO_2 nanocatalyst. *Nanoscale* **2010**, *2*, 1109−1111.

(39) Rajeshwar, K.; Osugi, M. E.; Chanmanee, W.; Chenthamarakshan, C. R.; Zanoni, M. V. B.; Kajitvichyanukul, P.; Krishnan-Ayer, R. Heterogeneous photocatalytic treatment of organic dyes in air and aqueous media. *J. Photochem. Photobiol., C* **2008**, *9*, 171−192.

(40) Solomon, R. V.; Lydia, I. S.; Merlin, J. P.; Venuvanalingam, P. Enhanced photocatalytic degradation of azo dyes using nano Fe_3O_4. *J. Iran. Chem. Soc.* **2012**, *9*, 101−109.

(41) Sarkar, S.; Makhal, A.; Bora, T.; Lakhsman, K.; Singha, A.; Dutta, J.; Pal, S. K. Hematoporphyrin−ZnO Nanohybrids: Twin Applications in Efficient Visible-Light Photocatalysis and Dye-Sensitized Solar Cells. *ACS Appl. Mater. Interfaces* **2012**, *4*, 7027−7035.

(42) Goswami, N.; Saha, R.; Pal, S. K. Protein-assisted synthesis route of metal nanoparticles: exploration of key chemistry of the biomolecule. *J. Nanopart. Res.* **2011**, *13*, 5485−5495.

(43) Sarkar, S.; Makhal, A.; Baruah, S.; Mahmood, M. A.; Dutta, J.; Pal, S. K. Nanoparticle-Sensitized Photodegradation of Bilirubin and Potential Therapeutic Application. *J. Phys. Chem. C* **2012**, *116*, 9608−9615.

(44) Lee, S.-K.; Mills, A. Novel photochemistry of leuco-Methylene Blue. *Chem. Commun.* **2003**, 2366−2367.

(45) Goswami, N.; Giri, A.; Kar, S.; Bootharaju, M. S.; John, R.; Xavier, P. L.; Pradeep, T.; Pal, S. K. Protein-Directed Synthesis of NIR-Emitting, Tunable HgS Quantum Dots and Their Applications in Metal-Ion Sensing. *Small* **2012**, *8*, 3175−3184.

(46) Katz, E.; Willner, I. Magneto-controlled Quantized Electron Transfer to Surface-confined Redox Units and Metal Nanoparticles. *Sensors* **2006**, *6*, 420−427.

(47) Yu, L.; Wu, H.; Wu, B.; Wang, Z.; Cao, H.; Fu, C.; Jia, N. Magnetic Fe_3O_4-Reduced Graphene Oxide Nanocomposites-Based Electrochemical Biosensing. *Nano-Micro Lett.* **2014**, *6*, 258−267.